24th INTERNATIONAL CONGRESS ON SOUND AND VIBRATION
23–27 July 2017, London

ICSV24
23-27JULY 2017
LONDON CALLING

ANALYSIS OF WAVE SCATTERING FROM NON-SYMMETRIC DISCONTINUITIES IN ONE-DIMENSIONAL WAVEGUIDES

Breno Takiuti, Vicente Lopes Junior, Michael Brennan

UNESP - São Paulo State University, Department of Mechanical Engineering, Ilha Solteira, BRAZIL
email: takiuti.breno@gmail.com

Elisabetta Manconi

University of Parma, Department of Engineering and Architecture, Parma, ITALY.

Predicting the scattering from waves that are incident on a damaged section of structure is of importance in structural health monitoring and nondestructive testing techniques to detect damage. High frequency waves are generally involved, and simple models which cannot capture the dynamic behaviour of the waveguides at high frequency, can result in experimental failure and misinterpretation of the results. Moreover, damage is generally non-symmetrical with respect to the neutral axis of the structure, resulting in wavemode conversion and different reflected and transmitted waves propagating with different velocities. The aim of this work is to investigate wave reflection and transmission over a wide frequency range due to non-symmetric discontinuities in a one-dimensional waveguide. These can be either fluid-filled pipes or plates or beams with point discontinuities or finite length damage. In this work, wave propagation analysis for the undamaged waveguide is carried out using the wave finite element method, where a small segment of the waveguide is modelled using a number of solid or plane elements which can describe both rich wave behaviour and wavemode conversion. Continuity and equilibrium conditions are imposed at the interfaces using a wave-matrix based approach and the scattering matrix is obtained, together with the power reflection and transmission ratios. These provide valuable information about the effect of damage on the propagating waves. A numerical example is presented which consists of a change of cross-sectional area.
Keywords: guided waves, wave scattering, finite elements, damage detection

1. Introduction

Structural health monitoring (SHM) consists of a set of techniques in which a given structure is monitored to avoid catastrophic accidents. By exciting the structure with a guided wave and analysing the reflected waves, a large part of the structure can be monitored, making this procedure ideal for damage detection in pipes, for example. Several authors have been studying damage detection techniques using waves, see for example [1-5].

SHM techniques can benefit from knowledge of the wave characteristics propagating in the structure: in order to identify the damage from a measured wave signal, the signal can be compared with that simulated from a computational model which can predict the behaviour of the damaged waveguide. A method for predicting wave characteristics is the wave and finite element (WFE) method, which uses periodic structure theory together with a finite element (FE) model of a small portion of the structure. The method has been applied to a number of benchmark cases, such as the vibration of tires [6], and free and forced wave propagation in cylindrical waveguides [7, 8] etc. Following some previous papers by Mace et al. [9, 10] where scattering of waves was studied, recently an hybrid

FE/WFE approach for the computation of the scattering properties of joints in waveguides has also been studied [11, 12].

In this paper, scattering of wave in a waveguide with a non-symmetric change in the cross-sectional area is studied by applying the WFE method. This kind of discontinuity, which can model, for example, damage due to corrosion [1], is difficult to be studied analytically since mode conversion and other complicating phenomena may occur, in particular at high frequency. The structure considered can represent one-dimensional waveguides such as beam, plates, cylindrical shells etc. A WFE numerical case is studied using standard FE plane elements to obtain dispersion curves and wavemodes which are subsequently used to find the scattering matrix and the reflection and transmission power coefficients. Comparison with analytical results for a symmetric change of area is first presented. Results for a non-symmetric change of area are then shown and mode conversion is discussed in terms of kinetic energy content in the *x* and *y* direction for the reflected and transmitted disturbances.

2. WFE Modelling of the Scattering Matrix

Consider two generic 1D waveguides **A** and **B** with a discontinuity as shown in Fig. 1. This discontinuity causes the traveling waves to scatter, generating reflected and transmitted waves. Waves can propagate in the right (positive) and the left (negative) direction in both waveguides. The vectors of wave amplitudes are denoted by $\mathbf{a}^+, \mathbf{a}^-$ and $\mathbf{b}^+, \mathbf{b}^-$. In the present study, the discontinuity represents a change in the cross-sectional area.

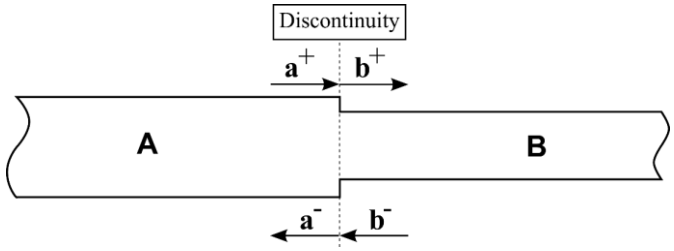

Figure 1: Wave reflection and transmission at the change of the cross section.

To find the scattering matrices, the vectors of waves **a** and **b** are described in terms of linear combinations of the wavemodes. These are obtained by solving the WFE eigenvalue problem as described in [6]. The vector of nodal displacements $\mathbf{q}_A$ and vector of nodal forces $\mathbf{f}_A$ for waveguide **A** are given by

$$\begin{Bmatrix} \mathbf{q}_A \\ \mathbf{f}_A \end{Bmatrix} = \begin{bmatrix} \mathbf{\Phi}^+_{q,A} & \mathbf{\Phi}^-_{q,A} \\ \mathbf{\Phi}^+_{f,A} & \mathbf{\Phi}^-_{f,A} \end{bmatrix} \begin{Bmatrix} \mathbf{a}^+ \\ \mathbf{a}^- \end{Bmatrix} \tag{1}$$

where $\mathbf{\Phi}$ is a matrix of wavemode shapes, $\mathbf{a}^+$ and $\mathbf{a}^-$ are the vectors of wave amplitudes in the positive and negative directions respectively, the subscripts f and q indicate wavemodes related to the nodal forces and displacements respectively, and the subscript a indicates the left waveguide in Fig. 1. The same equations can be written for the nodal displacements and forces of the right waveguide **B**. The equilibrium of forces and continuity of the displacements at the discontinuity can be written in vector-matrix form as

$$\mathbf{C}_A\mathbf{q}_A = \mathbf{C}_B\mathbf{q}_B; \quad \mathbf{D}_A\mathbf{f}_A = \mathbf{D}_B\mathbf{f}_B \tag{2a,b}$$

where **C** and **D** are matrices used to describe the boundary conditions at the discontinuity. Combining Eqs. (1) and (2), results in

$$\begin{Bmatrix} \mathbf{a}^{-} \\ \mathbf{b}^{+} \end{Bmatrix} = \mathbf{T}_{\mathbf{RT}} \begin{Bmatrix} \mathbf{a}^{+} \\ \mathbf{b}^{-} \end{Bmatrix} \tag{3}$$

where

$$\mathbf{T}_{\mathrm{RT}} = \begin{bmatrix} \mathbf{R}^{\mathrm{AA}} & \mathbf{T}^{\mathrm{AB}} \\ \mathbf{T}^{\mathrm{BA}} & \mathbf{R}^{\mathrm{BB}} \end{bmatrix} = \begin{bmatrix} \mathbf{C}_{\mathrm{A}}\boldsymbol{\Phi}^{-}_{\mathrm{q,A}} & -\mathbf{C}_{\mathrm{B}}\boldsymbol{\Phi}^{+}_{\mathrm{q,B}} \\ \mathbf{D}_{\mathrm{A}}\boldsymbol{\Phi}^{-}_{\mathrm{f,A}} & -\mathbf{D}_{\mathrm{B}}\boldsymbol{\Phi}^{+}_{\mathrm{f,B}} \end{bmatrix}^{-1} \begin{bmatrix} -\mathbf{C}_{\mathrm{A}}\boldsymbol{\Phi}^{+}_{\mathrm{q,A}} & \mathbf{C}_{\mathrm{B}}\boldsymbol{\Phi}^{-}_{\mathrm{q,B}} \\ -\mathbf{D}_{\mathrm{A}}\boldsymbol{\Phi}^{+}_{\mathrm{f,A}} & \mathbf{D}_{\mathrm{B}}\boldsymbol{\Phi}^{-}_{\mathrm{f,B}} \end{bmatrix} \tag{4}$$

is the wave scattering matrix. The time-averaged kinetic energy and the time-averaged energy flow can be also calculated using [13]

$$E^{\pm}_{flow} = \frac{1}{2}\mathrm{Re}\left[\left(\mathbf{a}^{\pm}\boldsymbol{\Phi}^{\pm}_{\mathrm{f,A}}\right)^{\mathrm{H}}(i\omega)\boldsymbol{\Phi}^{\pm}_{\mathrm{q,A}}\mathbf{a}^{\pm}\right]; \qquad E^{\pm}_{kin} = \frac{(i\omega)^2}{4}\mathrm{Re}\left[\left(\mathbf{a}^{\pm}\boldsymbol{\Phi}^{\pm}_{\mathrm{q,A}}\right)^{\mathrm{H}}\mathbf{M}_{\mathrm{A}}\boldsymbol{\Phi}^{\pm}_{\mathrm{q,A}}\mathbf{a}^{\pm}\right] \tag{5}$$

where **M** is the mass matrix of the section in which the time average kinetic energy is being calculated and the superscript H denotes the Hermitian matrix operator. The power matrix can be calculated in each waveguide by

$$\mathbf{P} = \frac{i\omega}{2}\left\{\begin{bmatrix} \boldsymbol{\Phi}_{\mathrm{q}}^{+\mathrm{H}}\boldsymbol{\Phi}_{\mathrm{f}}^{+} & \boldsymbol{\Phi}_{\mathrm{q}}^{+\mathrm{H}}\boldsymbol{\Phi}_{\mathbf{f}}^{-} \\ \boldsymbol{\Phi}_{\mathrm{q}}^{-\mathrm{H}}\boldsymbol{\Phi}_{\mathrm{f}}^{+} & \boldsymbol{\Phi}_{\mathrm{q}}^{-\mathrm{H}}\boldsymbol{\Phi}_{\mathrm{f}}^{-} \end{bmatrix} - \begin{bmatrix} \boldsymbol{\Phi}_{\mathrm{f}}^{+\mathrm{H}}\boldsymbol{\Phi}_{\mathrm{q}}^{+} & \boldsymbol{\Phi}_{\mathrm{f}}^{+\mathrm{H}}\boldsymbol{\Phi}_{\mathrm{q}}^{-} \\ \boldsymbol{\Phi}_{\mathrm{f}}^{-\mathrm{H}}\boldsymbol{\Phi}_{\mathrm{q}}^{+} & \boldsymbol{\Phi}_{\mathrm{f}}^{-\mathrm{H}}\boldsymbol{\Phi}_{\mathrm{q}}^{-} \end{bmatrix}\right\} \tag{6}$$

which is an *m* by *m* matrix, where *m* is the number of wavemodes [12]. The reflected and transmitted power coefficients can then be evaluated for a single wavemode using

$$\upsilon = \left|r^{\mathrm{AA}}\right|^2 \frac{P_{\mathrm{A}}^{\mathrm{rr}}}{P_{\mathrm{A}}^{\mathrm{ii}}}; \qquad \tau = \left|t^{\mathrm{BA}}\right|^2 \frac{P_{\mathrm{B}}^{\mathrm{tt}}}{P_{\mathrm{A}}^{\mathrm{ii}}} \tag{7}$$

where the superscripts i, r, and t in Eq. (7) represents the positions in the $\mathbf{P}$ matrix corresponding to the positive going wave in **A**, negative going wave in **A** and positive going wave in **B** respectively, the scalars r and t are reflection and transmission coefficients taken from submatrices $\mathbf{R}^{\mathrm{AA}}$, $\mathbf{R}^{\mathrm{BB}}$, $\mathbf{T}^{\mathrm{BA}}$ or $\mathbf{T}^{\mathrm{AB}}$ and P are scalars taken from the power matrix.

3. Numerical Results

This section shows some results for reflection and transmission of waves propagating in one-dimensional waveguides with a change in the cross-sectional area. The WFE method is applied and the waveguides are discretized using 2D standard FE plane element in plane stress, defined by four nodes, each node having two degrees of freedom: translations in the *x* and *y* directions. The FE matrices of a small segment of waveguides **A** and **B**, are obtained and the WFE modelling is applied to obtain the dispersion curves and wavemodes in each waveguide. In the numerical example three wavemodes are considered: bending propagating, longitudinal propagating and bending nearfield. The scattering matrix is then obtained as described in Section 2 once the boundary conditions are applied. The material properties are: density 7800kg/m^3, Young's modulus 206GPa, Poisson's ratio 0.3.

3.1 Symmetric change of area

Figure 2 depicts a schematic figure of the case considered, showing also the WFE discretization together with the geometrical properties.

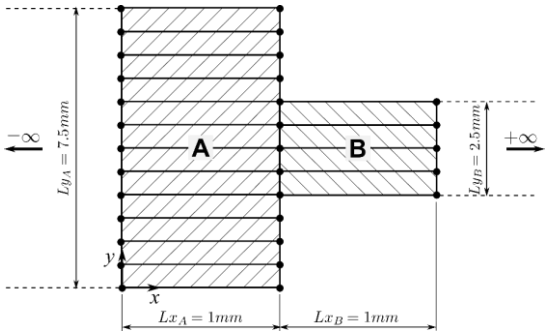

Figure 2: Symmetric discontinuity: WFE discretization using 12 plane elements for section **A** and 4 plane elements for section **B**.

Figure 3 shows the comparison between the dispersion curves obtained by the WFE and those obtained analytically for an equivalent beam in bending motion (Euler-Bernoulli beam) and a bar in axial motion. It can be seen that there is a large discrepancy at high frequency due to the Euler-Bernoulli model. In the following, wavemodes up to 200kHz are considered, therefore only the bending propagating, longitudinal propagating and bending nearfield waves are assumed here.

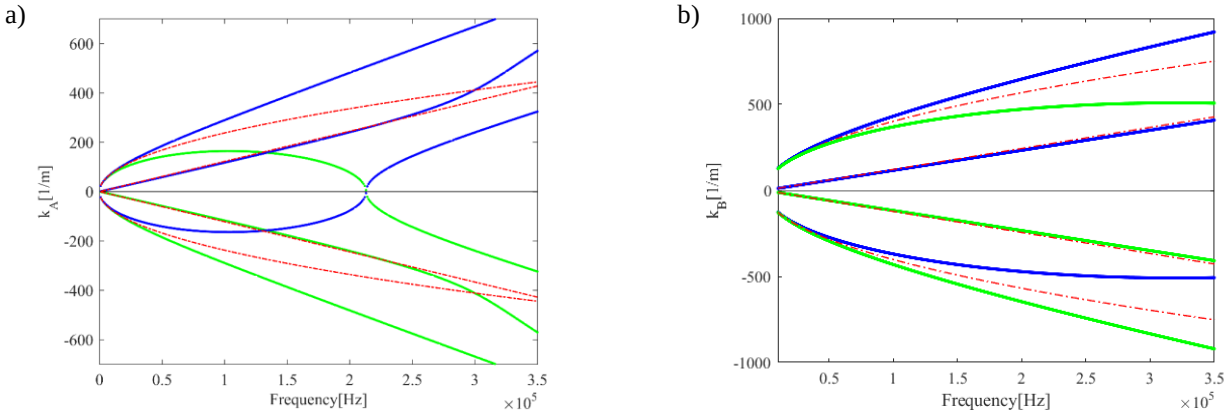

Figure 3: Complex dispersion curves: a) waveguide **A**; b) waveguide **B**. ——— WFE solutions: blue lines for positive going waves; green lines for negative going waves; –·–·– analytical solutions.

3.1.1 Incident bending and longitudinal propagating wave: reflection and transmission coefficients; comparison with analytical results.

Consider a bending propagating wave incident upon the change of the cross section. Figures 4 and 5 show the reflection and transmission coefficients for the reflected and transmitted bending and longitudinal waves. Results for the nearfield waves are omitted since they are decaying waves with no energy flow in the case considered (although these nearfield waves are important at the discontinuity). In Figs. 4 and 5 the reflection and transmission coefficients are compared with those obtained analytically. Results show that there is a very good agreement between the analytical and the results obtained from Eq. (4) for frequencies lower than about 50kHz. The difference in the absolute value of the transmission coefficient is due to the better FE description in terms of the nodal displacements in the two directions *x* and *y* at the discontinuity. Discrepancies at high frequency (>50kHz) are due to the differences in the models (failure of the analytical beam and bar model) as it can be also seen in Fig. 3.

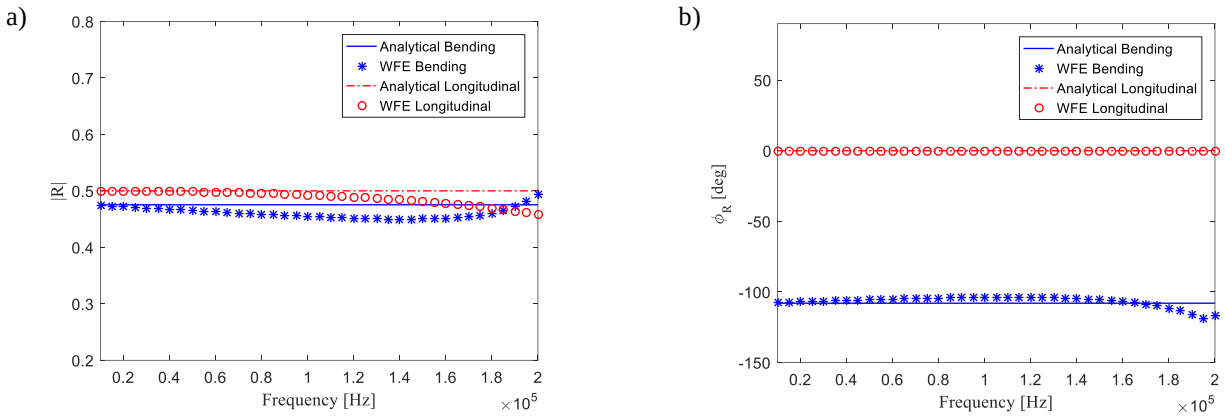

Figure 4: Symmetric change of cross-sectional area. Reflection coefficients: a) absolute value; b) phase.

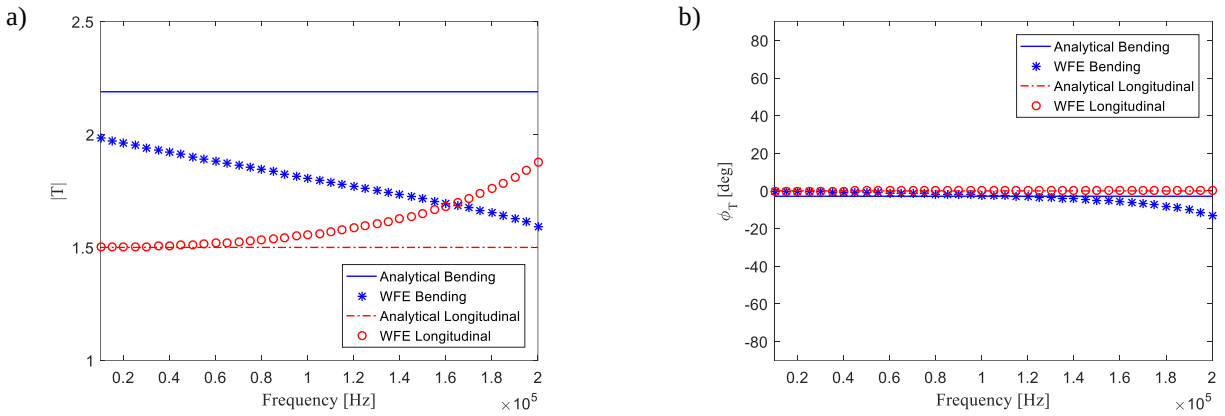

Figure 5: Symmetric change of cross-sectional area. Transmission coefficients: a) absolute value; b) phase.

3.1.2 Incident bending wave: power reflection and transmission coefficients and time-averaged kinetic energy

As an example, the results when a bending wave is incident are shown. Figure 6 shows the reflection and transmission power coefficients obtained using Eq. (7). Since there is no dissipation in the discontinuity the sum of the all reflected and transmitted power is one, as expected. It can be seen that only coefficients associated with the bending modes are greater than zero, and that the behaviour changes around the point in which the nearfield bending wavemode crosses the longitudinal wavemode in Fig. 3(a). Due to the symmetry, theoretically there is no wavemode conversion at the discontinuity. This can be evaluated easily considering the power reflection and transmission coefficients and the time-averaged kinetic energy content in the *x* and *y* directions with respect to the total time averaged kinetic energy for both reflected and transmitted waves. Figure 7(a) shows the percentage of the incident time-averaged kinetic energy in the *x* and *y* direction with respect to the total incident time-averaged kinetic energy associated with the bending wave. Figure 7(b) shows the reflected and transmitted time-averaged kinetic energy in the *x* and *y* direction with respect to the total reflected and transmitted time-averaged kinetic energy. It can be seen that as frequency increases, the percentage of the time-averaged kinetic energy in the *y* direction decreases and the percentage of the time-averaged kinetic energy in the *x* direction increases. In particular, it can be seen there is an exchange of the two behaviours around the frequency in which the nearfield bending dispersion curve crosses the longitudinal dispersion curve, see Fig. 3.

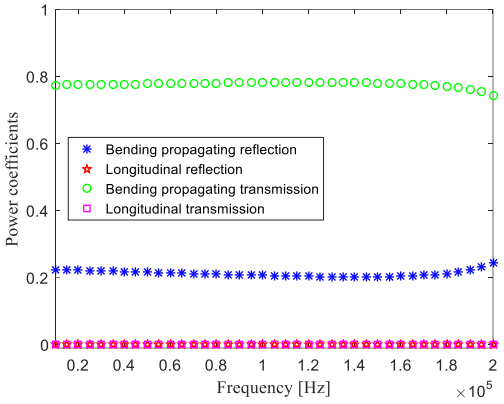

Figure 6: Symmetric change of cress-sectional area. Power reflection and transmission coefficients.

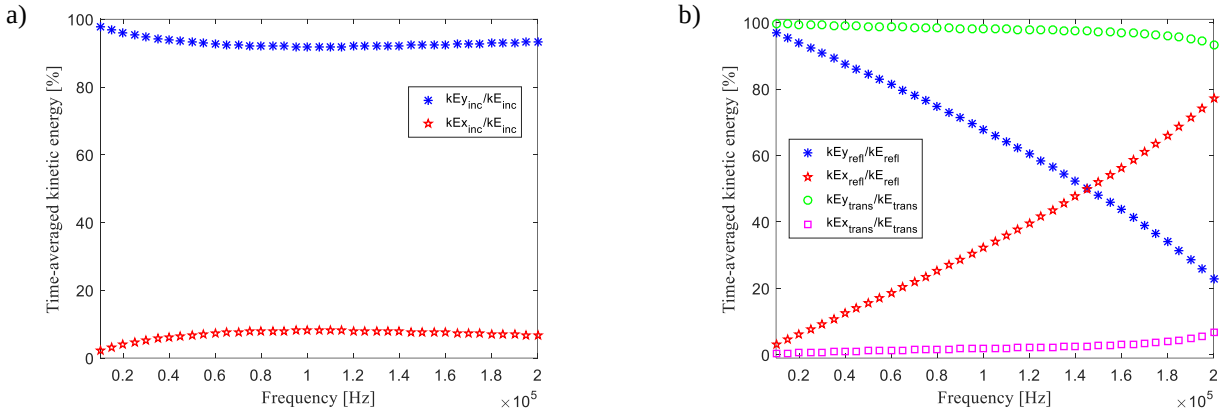

Figure 7: Symmetric change of cross-sectional area. Percentage of the time-averaged kinetic energy in the *x* and *y* direction with respect to the total time-averaged kinetic energy: a) incident bending wave, b) reflected and transmitted waves

3.2 Non-symmetric change of area

In this section the results in terms of power reflection and transmission coefficients and time-averaged kinetic energy are shown for a non-symmetrical change of area, as depicted in Fig. 8. Two cases are considered as shown in Figs. 8(a) and 8(b). These are referred to as case 1 and case 2.

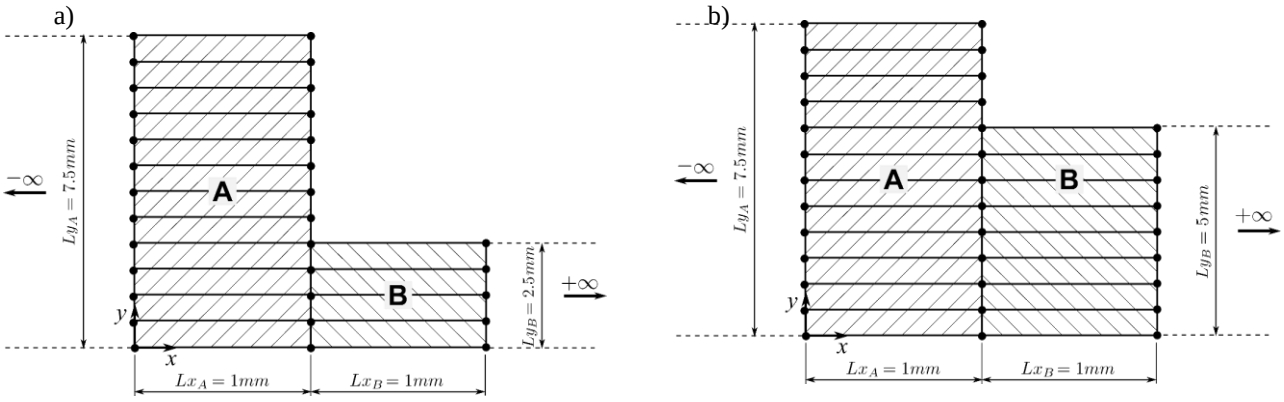

Figure 8: Non-symmetric discontinuity: a) case 1; b) case 2.

3.2.1 Incident bending wave: power reflection and transmission coefficients and time-averaged kinetic energy

Consider a pure bending propagating wave incident upon the non-symmetric discontinuity. Figure 9 shows the reflected and transmitted power coefficients, while Fig. 10 shows the reflected and

transmitted time-averaged kinetic energy in the *x* and *y* directions with respect to the total reflected and transmitted time-averaged kinetic energy. Compared to the previous case it can be seen that, in the frequency range considered, there is a significant mode conversion for case 1 and almost no reflection for case 2. Comparing Fig. 9 with Fig. 6, it can be seen that the power coefficients for the longitudinal reflected and transmitted modes are greater than zero for case 1, while almost all the energy flow associated with the incident bending wave is transmitted for case 2. In particular Fig. 9(b) shows that higher frequencies (shorter wavelength), must be considered to evaluate the reflection in case 2. Considering the percentage of the time-averaged kinetic energy in the *x* and *y* direction, Figs. 10(a) and (b) show that the reflected and transmitted waves have different energy contents in the *x* and *y* directions for both case 1 and 2 with respect to an incident bending wave as showed in Fig. 7(a). This shows a change in the cross-sectional displacements for the reflected and transmitted waves with respect to the nature of the incident wave.

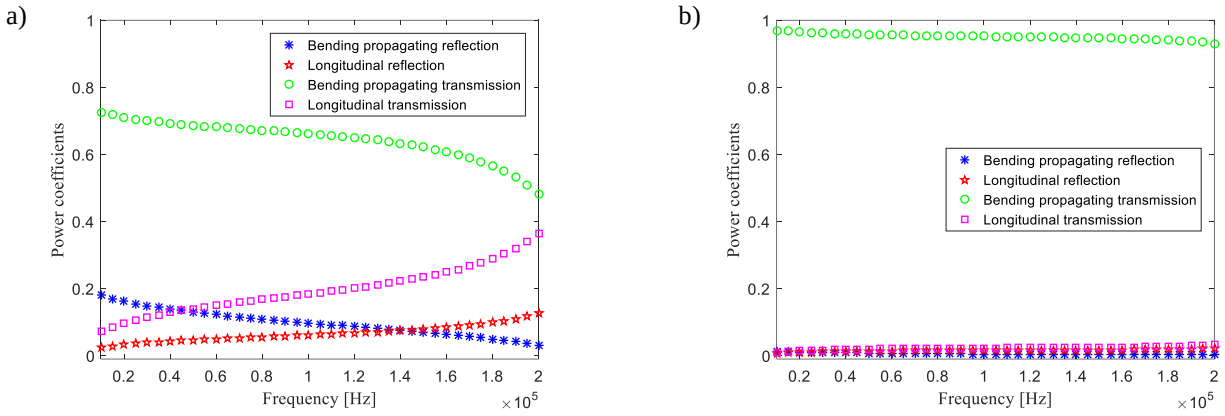

Figure 9: Non-symmetric change of cross-sectional area. Power reflection and transmission coefficients for case 1, (a), and case 2, (b).

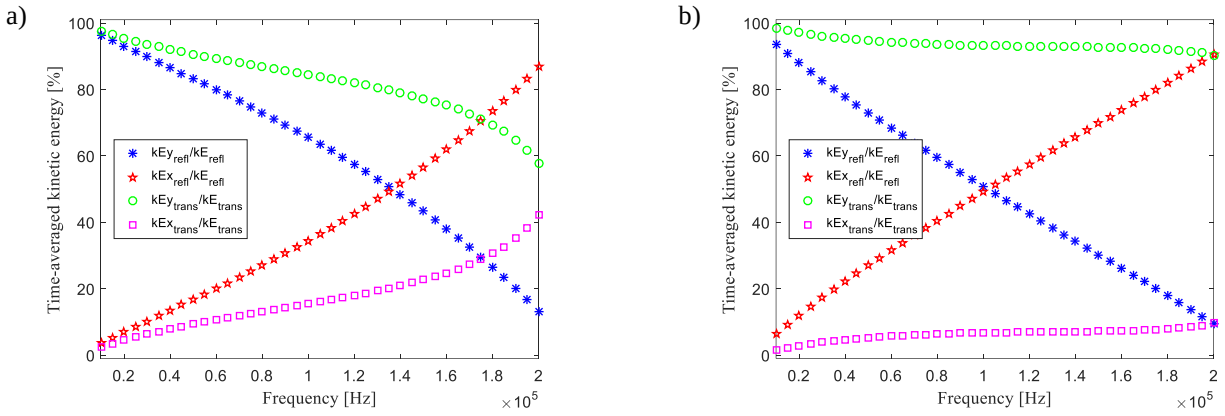

Figure 10: Non-symmetric change of cross-sectional area. Percentage of the time-averaged kinetic energy in the *x* and *y* direction with respect to the total time-averaged kinetic for case 1, (a), and case 2, (b).

4. Conclusions

In this paper, the scattering of waves induced by an incident wavefield on a change in cross-section of a one-dimensional waveguide is modelled using a wave matrix approach. A WFE model is applied to determine the wavemodes using FE plane elements discretized through the cross-section of the waveguides. This model can describe both rich wave behaviour and wavemode conversion. Results are given in terms of the reflection and transmission coefficients and in terms of the energy content in the reflected and transmitted disturbances up to high frequency. At low frequency, comparison between the numerical results and those obtained by an analytical model in the case of a

symmetric change of area has shown that the method can predict scattering with very good accuracy. Scattering in the case of a non-symmetric change of cross-sectional area is shown in terms of power reflection and transmission coefficients and energy content in the reflected and transmitted disturbances. The approach has been seen to be efficient in modelling wave reflection and transmission, and the intention is to use it to investigate the wave scattering from symmetric and non-symmetric damages. Deeper investigation of wave scattering behaviour at high frequency, including higher order wavemode, is the subject of on-going work.

REFERENCES

1 Demma, A., Cawley, P., Lowe, M., Roosenbrand, A. G. and Pavlakovic, B. The reflection of guided waves from notches in pipes: a guide for interpreting corrosion measurements, *NDT & E International*, **37** (3), 167-180, (2004).
2 Lowe, M. J. S., Alleyne, D. N. and Cawley, P. Defect detection in pipes using guided waves, *Ultrasonics*, **36** (1), 147-154, (1998).
3 Muggleton, J. M., Brennan, M. J. and Pinnington, R. J. Wavenumber prediction of waves in buried pipes for water leak detection, *Journal of Sound and Vibration*, **249** (5), 939-954, (2002).
4 Staszewski, W. J., Pierce, S. G., Worden, K., Philp, W. R., Tomlinson, G. R. and Culshaw, B. Wavelet signal processing for enhanced Lamb-wave defect detection in composite plates using optical fiber detection, *Optical Engineering*, **36** (7), 1877-1888, (1997).
5 Brennan, M. J., Elliott, S. J. and Pinnington, R. J. The dynamic coupling between piezoceramic actuators and a beam, *The Journal of the Acoustical Society of America*, **102** (4), 1931-1942, (1997).
6 Waki, Y., Mace, B. R. and Brennan, M. J. Free and forced vibrations of a tyre using a wave/finite element approach, *Journal of Sound and Vibration*, **323** (3–5), 737-756, (2009).
7 Manconi, E. and Mace, B. R. Wave characterization of cylindrical and curved panels using a finite element method, *The Journal of the Acoustical Society of America*, **125** (1), 154-163, (2009).
8 Renno, J. M. and Mace, B. R. Calculating the forced response of cylinders and cylindrical shells using the wave and finite element method, *Journal of Sound and Vibration*, **333** (21), 5340-5355, (2014).
9 Harland, N. R., Mace, B. R. and Jones, R. W. Wave propagation, reflection and transmission in tunable fluid-filled beams, *Journal of Sound and Vibration*, **241** (5), 735-754, (2001).
10 Mace, B. R., Jones, R. W. and Harland, N. R. Wave transmission through structural inserts, *The Journal of the Acoustical Society of America*, **109** (4), 1417-1421, (2001).
11 Renno, J. M. and Mace, B. R. Calculation of reflection and transmission coefficients of joints using a hybrid finite element/wave and finite element approach, *Journal of Sound and Vibration*, **332** (9), 2149-2164, (2013).
12 Mitrou, G., Ferguson, N. and Renno, J. Wave transmission through two-dimensional structures by the hybrid FE/WFE approach, *Journal of Sound and Vibration*, **389**, 484-501, (2017).
13 Mace, B. R., Duhamel, D., Brennan, M. J. and Hinke, L. Finite element prediction of wave motion in structural waveguides, *The Journal of the Acoustical Society of America*, **117** (5), 2835-2843, (2005).